Influence of Propeller Blade Lift Distribution on Whirl Flutter Stability Characteristics

J. Cecrdle

Abstract—This paper deals with the whirl flutter of the turboprop aircraft structures. It is focused on the influence of the blade lift span-wise distribution on the whirl flutter stability. Firstly it gives the overall theoretical background of the whirl flutter phenomenon. After that the propeller blade forces solution and the options of the blade lift modeling are described. The problem is demonstrated on the example of a twin turboprop aircraft structure. There are evaluated the influences with respect to the propeller aerodynamic derivatives and finally the influences to the whirl flutter speed and the whirl flutter margin respectively.

Keywords—Aeroelasticity, flutter, propeller blade force, whirl flutter.

I. Introduction

AIRCRAFT structures are required to have a reliability certificate including the flutter stability. Flutter is a dynamic aeroelastic phenomenon occurring due to the interaction of unsteady aerodynamic, inertial and elastic forces emerging during the relative movement of the air and a flexible aircraft. Turboprop aircraft are required to be certified also considering the whirl flutter. The whirl flutter (also called gyroscopic flutter) that was discovered by Taylor and Browne [1] is the specific case of the flutter that includes additional dynamic and aerodynamic influences of the engine rotating parts. Rotating parts like a propeller or a gas turbine engine rotor increase the number of degrees of freedom and cause additional forces and moments. Moreover rotating propeller causes a complicated flow field and interference effects between wing, nacelle and propeller. The essential fact is an unsymmetric distribution of forces on a transversely vibrating propeller. Whirl flutter may cause a propeller mounting unstable vibrations, even a failure of an engine, nacelle or whole wing. It has been the cause of a number of accidents.

II. Theoretical Background

The fundamental solution [2] is derived for the system with 2 degrees of freedom. Engine system flexible mounting can be substituted by the system of two rotational springs (stiffness K_Ψ, K_Θ) as illustrated in Fig. 1. Propeller is considered as rigid, rotating with angular velocity Ω. System is exposed to the airflow of velocity V∞.

Neglecting the propeller rotation and the aerodynamic forces, the two independent mode shapes will emerge with angular frequencies ω_Ψ and ω_Θ. Considering the propeller

J. Cecrdle is with the Aeronautical Research and Test Institute (VZLU), Prague, Czech Republic (phone: +420 225115123; fax: +420 283920018; e-mail: cecrdle@vzlu.cz).

rotation, the primary system motion changes to the characteristic gyroscopic motion. The gyroscopic effect makes two independent mode shapes merge to whirl motion. The propeller axis shows an elliptical movement. The orientation of the propeller axis movement is backward relative to the propeller rotation for the mode with lower frequency (backward whirl mode) and forward relatively to the propeller rotation for the mode with higher frequency (forward whirl mode). The mode shapes of gyroscopic modes are complex, since independent yaw and pitch modes have a phase shift 90°.
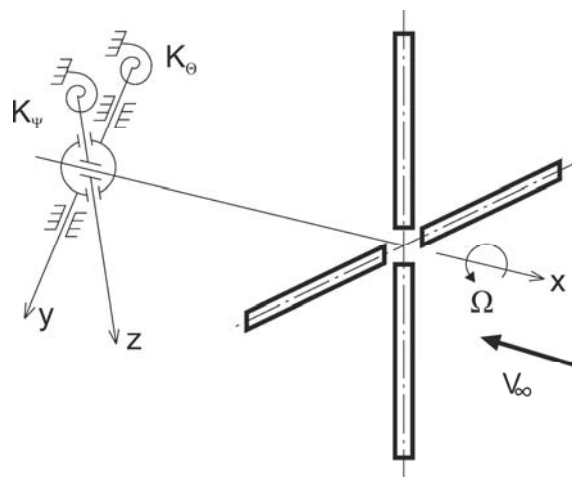

Fig. 1 Gyroscopic system with propeller

The described gyroscopic mode shapes cause harmonic changes of propeller blades angles of attack. They give rise to unsteady aerodynamic forces, which may under the specific conditions induce a whirl flutter. Possible states of the gyroscopic system from the flutter stability point of view for backward mode are explained in Fig. 2. Provided that the air velocity is lower than critical value ($V_\infty < V_{FL}$), the system is stable and the motion is damped. If the airspeed exceeds the critical value ($V_\infty > V_{FL}$), the system becomes unstable and motion is diverging. The state of the neutral stability ($V_\infty = V_{FL}$) with no total damping is called critical flutter state and V_{FL} is called critical flutter speed.

The basic problem of the analytical solution consists in the determination of the aerodynamic forces caused by the gyroscopic motion for the specific propeller blades. The equations of motion were set up for the system described in Fig. 1. The kinematical scheme including gyroscopic effects [3] is shown in Fig. 3. The independent generalized coordinates are three angles (φ, Θ, Ψ). We assume the propeller angular velocity constant ($\varphi = \Omega t$), mass distribution

World Academy of Science, Engineering and Technology
International Journal of Aerospace and Mechanical Engineering
Vol:8, No:4, 2014

symmetric around X-axis and mass moments of inertia $J_Z \neq J_Y$.
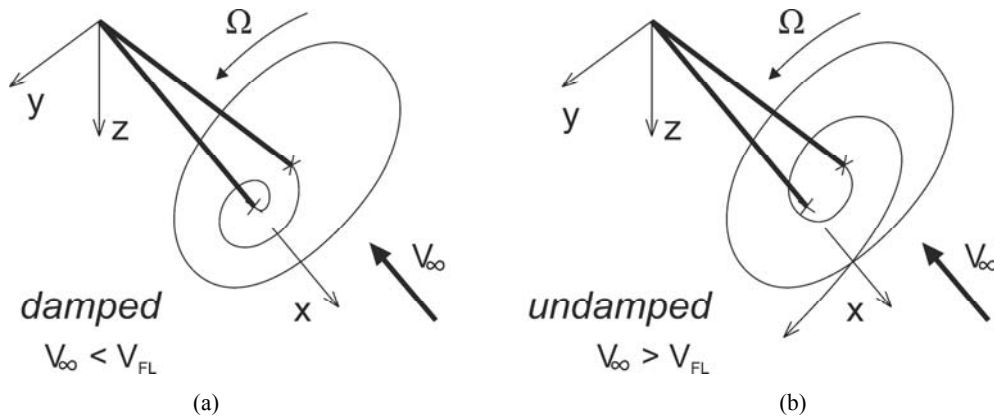

(a)   (b)

Fig. 2 Stable (a) and unstable (b) state of gyroscopic vibrations for backward flutter mode

Considering the small angles $(sin(x) \approx 0 \, ; \, cos(x) \approx 1)$ the equations of motion become:

$$J_Y \ddot{\Theta} + \frac{K_\Theta \gamma_\Theta}{\omega} \dot{\Theta} + J_X \Omega \dot{\Psi} + K_\Theta \Theta = M_{Y,P} - a.P_Z$$
$$J_Z \ddot{\Psi} + \frac{K_\Psi \gamma_\Psi}{\omega} \dot{\Psi} - J_X \Omega \dot{\Theta} + K_\Psi \Psi = M_{Z,P} + a.P_Y \qquad (1)$$

We formulate the propeller aerodynamic forces by means of the aerodynamic derivatives as described in Section III and make the simplification for the harmonic motion, then the final whirl flutter matrix equation become:

$$\left(-\omega^2 [M] + j\omega \left([D] + [G] + q_\infty F_P \frac{D_P^2}{V_\infty} [D^A] \right) + \left([K] + q_\infty F_P D_P [K^A] \right) \right) \begin{bmatrix} \bar{\Theta} \\ \bar{\Psi} \end{bmatrix} = \{0\} \qquad (2)$$

The limit state emerges for the specific combination of parameters V_∞ and Ω, when the angular velocity ω is real. Increasing the propeller advance ratio ($V_\infty / (\Omega R)$) requires an increase of the necessary stiffnesses; K_Θ, K_Ψ. Also influences

of the structural damping and the distance propeller – mode shape node are significant.

The whirl flutter appears at the gyroscopic rotational vibrations, the flutter frequency is the same as the frequency of the backward gyroscopic mode. The critical state may be reached either due to increasing the air velocity or the propeller revolutions. Structural damping is a significant stabilization factor. On the contrary, the propeller thrust influence is barely noticeable. The most critical state is $K_\Theta = K_\Psi$, it means $\omega_\Theta = \omega_\Psi$ when the interaction of both independent motions is maximal. A special case of (2) for $\omega = 0$ is the gyroscopic static divergence.

III. PROPELLER AERODYNAMIC FORCES

The fundamental solution of the propeller aerodynamic forces (right hand side of (1)) employing the Strip Theory [4], [5] for the rigid propeller blades was derived by Ribner [6], [7]. Later on the modified solution of Houbolt and Reed [8] became available as well. The propeller aerodynamic forces are expressed as:
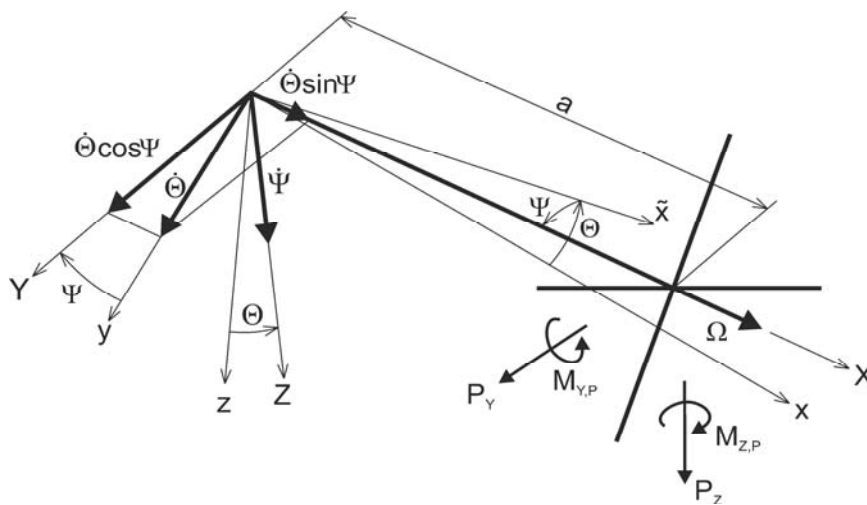

Fig. 3 Kinematical scheme of the gyroscopic system

World Academy of Science, Engineering and Technology
International Journal of Aerospace and Mechanical Engineering
Vol:8, No:4, 2014

$$P_Y = \pi \rho V_\infty^2 R^2 \left(c_{y\Theta}\Theta^* + c_{y\Psi}\Psi^* + c_{yq}\frac{\dot{\Theta}^* R}{V_\infty} + c_{yr}\frac{\dot{\Psi}^* R}{V_\infty} \right)$$

$$P_Z = \pi \rho V_\infty^2 R^2 \left(c_{z\Theta}\Theta^* + c_{z\Psi}\Psi^* + c_{zq}\frac{\dot{\Theta}^* R}{V_\infty} + c_{zr}\frac{\dot{\Psi}^* R}{V_\infty} \right) \quad (3)$$

$$M_{Y,P} = 2\pi \rho V_\infty^2 R^3 \left(c_{m\Theta}\Theta^* + c_{m\Psi}\Psi^* + c_{mq}\frac{\dot{\Theta}^* R}{V_\infty} + c_{mr}\frac{\dot{\Psi}^* R}{V_\infty} \right)$$

$$M_{Z,P} = 2\pi \rho V_\infty^2 R^3 \left(c_{n\Theta}\Theta^* + c_{n\Psi}\Psi^* + c_{nq}\frac{\dot{\Theta}^* R}{V_\infty} + c_{nr}\frac{\dot{\Psi}^* R}{V_\infty} \right)$$

where ρ is the air density and **R** is a propeller diameter. The effective angles are basically expressed as the quasi-steady values:

$$\Theta^* = \Theta + \frac{\dot{Z}}{V_\infty}$$

$$\Psi^* = \Psi - \frac{\dot{Y}}{V_\infty} \quad (4)$$

the c_{ij} terms represent the aerodynamic derivatives defined as:

$$c_{y\Theta} = \frac{\partial c_y}{\partial \Theta^*} \qquad c_{y\Psi} = \frac{\partial c_y}{\partial \Psi^*}$$

$$c_{yq} = \frac{\partial c_y}{\partial \left(\frac{\dot{\Theta} R}{V_\infty}\right)} \qquad c_{yr} = \frac{\partial c_y}{\partial \left(\frac{\dot{\Psi} R}{V_\infty}\right)}$$

$$c_{z\Theta} = \frac{\partial c_z}{\partial \Theta^*} \qquad c_{z\Psi} = \frac{\partial c_z}{\partial \Psi^*}$$

$$c_{zq} = \frac{\partial c_z}{\partial \left(\frac{\dot{\Theta} R}{V_\infty}\right)} \qquad c_{zr} = \frac{\partial c_z}{\partial \left(\frac{\dot{\Psi} R}{V_\infty}\right)}$$

$$c_{m\Theta} = \frac{\partial c_m}{\partial \Theta^*} \qquad c_{m\Psi} = \frac{\partial c_m}{\partial \Psi^*}$$

$$c_{mq} = \frac{\partial c_m}{\partial \left(\frac{\dot{\Theta} R}{V_\infty}\right)} \qquad c_{mr} = \frac{\partial c_m}{\partial \left(\frac{\dot{\Psi} R}{V_\infty}\right)}$$

$$c_{n\Theta} = \frac{\partial c_n}{\partial \Theta^*} \qquad c_{n\Psi} = \frac{\partial c_n}{\partial \Psi^*}$$

$$c_{nq} = \frac{\partial c_n}{\partial \left(\frac{\dot{\Theta} R}{V_\infty}\right)} \qquad c_{nr} = \frac{\partial c_n}{\partial \left(\frac{\dot{\Psi} R}{V_\infty}\right)} \quad (5)$$

Note that we neglected the aerodynamic inertia terms in (5) as:

$$\dot{\Theta}^* \approx \dot{\Theta} \; ; \; \dot{\Psi}^* \approx \dot{\Psi} \quad (6)$$

further simplification comes with respect to the symmetry as:

$$c_{z\Psi} = c_{y\Theta} \; ; \; c_{m\Psi} = -c_{n\Theta} \; ; \; c_{mq} = c_{nr} \; ; \; c_{zr} = c_{yq} \; ;$$

$$c_{z\Theta} = -c_{y\Psi} \; ; \; c_{n\Psi} = c_{m\Theta} \; ; \; c_{mr} = -c_{nq} \; ; \; c_{yr} = -c_{zq} \quad (7)$$

and finally neglecting those ones with low values we can consider:

$$c_{mr} = -c_{nq} = 0 \; ; \; c_{yr} = -c_{zq} = 0 \quad (8)$$

In fact we have 6 independent values of aerodynamic derivatives. The derivatives are expressed by means of the propeller blade integrals that integrate the aerodynamic forces in the blade spanwise direction. The formulation of the integrals depends on the propeller geometric and aerodynamic characteristics. The basic formulation is given by Houbolt and Reed in [8] as:

$$A_1 = \int_0^1 \frac{c_0}{c_r} \frac{\mu^2}{\sqrt{\mu^2 + \eta^2}} d\eta$$

$$A_2 = \int_0^1 \frac{c_0}{c_r} \frac{\mu \eta^2}{\sqrt{\mu^2 + \eta^2}} d\eta \quad (9)$$

$$A_3 = \int_0^1 \frac{c_0}{c_r} \frac{\eta^4}{\sqrt{\mu^2 + \eta^2}} d\eta$$

This formulation is limited to the 4-blade propeller and theoretical blade lift curve slope ($a_0 = 2\pi$). It includes only 3 integrals accounting for the in-phase aerodynamic effects. It neglects the aerodynamic lift lag effects as well as the further important aerodynamic effects.

The extended formulation of the blade integrals is presented by Rodden and Rose [9]. It includes the aerodynamic lift lag effect by means of the Theodorsen function as proposed in [8]. The Theodorsen function terms are calculated by means of the Bessel functions first and second kind, zero and first order as:

$$F(k) = \frac{Bj_1(Bj_1 + By_0) + By_1(By_1 - Bj_0)}{(Bj_1 + By_0)^2 + (By_1 - Bj_0)^2}$$

$$G(k) = -\frac{By_1 By_0 + Bj_1 Bj_0}{(Bj_1 + By_0)^2 + (By_1 - Bj_0)^2} \quad (10)$$

where the blade section local reduced frequency k_p is expressed as:

$$k_P = \frac{c}{2R\sqrt{\mu^2 + \eta^2}} \quad (11)$$

where dimensionless propeller advance ratio is expressed as:

$$\mu = \frac{V_\infty}{\Omega R} \quad (12)$$

the dimensionless propeller radius is expressed as:

World Academy of Science, Engineering and Technology
International Journal of Aerospace and Mechanical Engineering
Vol:8, No:4, 2014

$$\eta = \frac{r}{R} \qquad (13)$$

and finally c and r are the blade local section chord and radius respectively.

The formulation of [9] also includes the correction to the compressibility by means of the Prandtl - Glauert correction considering the local blade section resultant Mach number M_r coming from the blade resultant velocity $\sqrt{V_\infty^2 + \Omega^2 r^2}$.

The Prandtl - Glauert correction factor is:

$$\frac{1}{\sqrt{1 - M_r^2}} \qquad (14)$$

Other correction factor accounting for the compressible flow blade aspect - ratio effect is expressed as:

$$\frac{A_r \sqrt{1 - M_r^2}}{2 + A_r \sqrt{1 - M_r^2}} \qquad (15)$$

Note that these corrections are included into the final blade integrals in the more appropriate form using the forward flight Mach number (M).

In the practical applications the integration range includes only the thrusting part of the propeller; therefore, the lower limit of the integration is shifted to the propeller boss radius r_0 which is in the dimensionless form expressed as:

$$\eta_0 = \frac{r_0}{R} \qquad (16)$$

In this case the blade aspect ratio is expressed as:

$$A_r = \frac{R}{c_r} \frac{(1 - \eta_0)^2}{\int_{\eta_0}^{1} \left(\frac{c}{c_r}\right) d\eta} \qquad (17)$$

where c_r is the blade reference chord.

The final correction of $(N_b/4)$ is applied to account for the number of blades N_b. Note that the solution is valid for the propellers of 3 or more blades that are considered as axisymmetric.

Applying the described corrections the number of the blade integrals is doubled comparing to (9). The $I_{(1-3)}$ are "in-phase" integrals including the $F(k)$ component of the Theodorsen function whereas $J_{(1-3)}$ are "out-of-phase" integrals including the $G(k)$ component. The corrected blade integrals are expressed as:

$$I_1 = \left(\frac{N_b}{4}\right)\left(\frac{a_0}{2\pi}\right)\frac{\mu^2 A_r}{c_r} \int_{\eta_0}^{1} \frac{c(\eta)\, F(k_P)}{\sqrt{\mu^2 + \eta^2}\left[2 + A_r \sqrt{1 - M^2\left(1 + \frac{\eta^2}{\mu^2}\right)}\right]} d\eta$$

$$J_1 = \left(\frac{N_b}{4}\right)\left(\frac{a_0}{2\pi}\right)\frac{\mu^2 A_r}{c_r} \int_{\eta_0}^{1} \frac{c(\eta)\, G(k_P)}{\sqrt{\mu^2 + \eta^2}\left[2 + A_r \sqrt{1 - M^2\left(1 + \frac{\eta^2}{\mu^2}\right)}\right]} d\eta$$

$$I_2 = \left(\frac{N_b}{4}\right)\left(\frac{a_0}{2\pi}\right)\frac{\mu A_r}{c_r} \int_{\eta_0}^{1} \frac{\eta^2 c(\eta)\, F(k_P)}{\sqrt{\mu^2 + \eta^2}\left[2 + A_r \sqrt{1 - M^2\left(1 + \frac{\eta^2}{\mu^2}\right)}\right]} d\eta$$

$$J_2 = \left(\frac{N_b}{4}\right)\left(\frac{a_0}{2\pi}\right)\frac{\mu A_r}{c_r} \int_{\eta_0}^{1} \frac{\eta^2 c(\eta)\, G(k_P)}{\sqrt{\mu^2 + \eta^2}\left[2 + A_r \sqrt{1 - M^2\left(1 + \frac{\eta^2}{\mu^2}\right)}\right]} d\eta$$

$$I_3 = \left(\frac{N_b}{4}\right)\left(\frac{a_0}{2\pi}\right)\frac{A_r}{c_r} \int_{\eta_0}^{1} \frac{\eta^4 c(\eta)\, F(k_P)}{\sqrt{\mu^2 + \eta^2}\left[2 + A_r \sqrt{1 - M^2\left(1 + \frac{\eta^2}{\mu^2}\right)}\right]} d\eta$$

$$J_3 = \left(\frac{N_b}{4}\right)\left(\frac{a_0}{2\pi}\right)\frac{A_r}{c_r} \int_{\eta_0}^{1} \frac{\eta^4 c(\eta)\, G(k_P)}{\sqrt{\mu^2 + \eta^2}\left[2 + A_r \sqrt{1 - M^2\left(1 + \frac{\eta^2}{\mu^2}\right)}\right]} d\eta$$

$$(18)$$

and the aerodynamic derivatives are expressed as:

$$c_{z\Theta} = -\left(\frac{4\Omega c_r}{V_\infty}\right) I_1 \qquad c_{zq} = \left(\frac{4\Omega c_r}{V_\infty}\right) J_2$$

$$c_{m\Theta} = -\left(\frac{2\Omega c_r}{V_\infty}\right) J_2 \qquad c_{mq} = -\left(\frac{2\Omega c_r}{V_\infty}\right) I_3$$

$$c_{y\Theta} = -\left(\frac{4\Omega c_r}{V_\infty}\right) J_1 \qquad c_{yq} = -\left(\frac{4\Omega c_r}{V_\infty}\right) I_2$$

$$c_{n\Theta} = -\left(\frac{2\Omega c_r}{V_\infty}\right) I_2 \qquad c_{nq} = -\left(\frac{2\Omega c_r}{V_\infty}\right) J_3$$

$$(19)$$

Equation (18) includes also the correction for the propeller lift curve slope (a_0) that is the parameter the paper is focused on. The lift curve slope that is defined as the derivative of the propeller force with respect to the effective angle of attack may be included as:

A. Profile Theoretical Value: $a_0 = 2\pi$

This is the basic option that is used in (9). It is used provided no information regarding the propeller aerodynamics is available.

B. Effective Value: $a_0 = a_{0eff}$

This is the option that is used in (19) by means of the factor $(a_0/2\pi)$. The effective value is the spanwise constant value that may be extracted from the spanwise lift slope distribution. In the most cases the $a_{0eff} < 2\pi$ therefore it ordinarily generates lower blade forces with the stabilizing outcome comparing to the former option.

World Academy of Science, Engineering and Technology
International Journal of Aerospace and Mechanical Engineering
Vol:8, No:4, 2014

C. Real Spanwise Distribution: $a_0 = a_0(\eta)$

This option is the most precise since it accounts for the real propeller force distribution. Ordinarily the root part of the blade generates quite low lift, the maximal lift is generated at about *3/4* of the blade span and again the tip region generates lower lift. The lift curve slope distribution may be variable considering specific types of propellers. Optionally the typical distributions which are presented e.g. in [10] may be employed.

Considering the spanwise variable lift curve slope the a_0 moves under the integrand and the propeller blade integrals of (18) change into the form of:

$$I_1 = \left(\frac{N_b}{4}\right)\left(\frac{1}{2\pi}\right)\frac{\mu^2 A_r}{c_r}\int_{\eta_0}^{1}\frac{a_0(\eta)c(\eta)F(k_P)}{\sqrt{\mu^2+\eta^2}\left[2+A_r\sqrt{1-M^2\left(1+\frac{\eta^2}{\mu^2}\right)}\right]}d\eta$$

$$J_1 = \left(\frac{N_b}{4}\right)\left(\frac{1}{2\pi}\right)\frac{\mu^2 A_r}{c_r}\int_{\eta_0}^{1}\frac{a_0(\eta)c(\eta)G(k_P)}{\sqrt{\mu^2+\eta^2}\left[2+A_r\sqrt{1-M^2\left(1+\frac{\eta^2}{\mu^2}\right)}\right]}d\eta$$

$$I_2 = \left(\frac{N_b}{4}\right)\left(\frac{1}{2\pi}\right)\frac{\mu A_r}{c_r}\int_{\eta_0}^{1}\frac{\eta^2 a_0(\eta)c(\eta)F(k_P)}{\sqrt{\mu^2+\eta^2}\left[2+A_r\sqrt{1-M^2\left(1+\frac{\eta^2}{\mu^2}\right)}\right]}d\eta$$

$$J_2 = \left(\frac{N_b}{4}\right)\left(\frac{1}{2\pi}\right)\frac{\mu A_r}{c_r}\int_{\eta_0}^{1}\frac{\eta^2 a_0(\eta)c(\eta)G(k_P)}{\sqrt{\mu^2+\eta^2}\left[2+A_r\sqrt{1-M^2\left(1+\frac{\eta^2}{\mu^2}\right)}\right]}d\eta$$

$$I_3 = \left(\frac{N_b}{4}\right)\left(\frac{1}{2\pi}\right)\frac{A_r}{c_r}\int_{\eta_0}^{1}\frac{\eta^4 a_0(\eta)c(\eta)F(k_P)}{\sqrt{\mu^2+\eta^2}\left[2+A_r\sqrt{1-M^2\left(1+\frac{\eta^2}{\mu^2}\right)}\right]}d\eta$$

$$J_3 = \left(\frac{N_b}{4}\right)\left(\frac{1}{2\pi}\right)\frac{A_r}{c_r}\int_{\eta_0}^{1}\frac{\eta^4 a_0(\eta)c(\eta)G(k_P)}{\sqrt{\mu^2+\eta^2}\left[2+A_r\sqrt{1-M^2\left(1+\frac{\eta^2}{\mu^2}\right)}\right]}d\eta$$

(20)

Note that the further correction of the blade lift slope is the cut-off value in the transonic flow that is applied to avoid the Mach number correction for the blade tip supersonic speed (e.g. condition of the propeller overspeed etc.). With regard to the fact that this correction can be applied regardless the lift curve slope model it is not included to the presented evaluation.

The described options, in particular the two latter ones are compared with respect to the aerodynamic derivatives and the flutter stability in the next section.

IV. APPLICATION EXAMPLE

The evaluation is performed on the structure of the EV-55M aircraft that is ordinary twin tractor turboprop for *9-13* passengers with the total length of *14.35m*, the wingspan of *16.10m* and the maximal take-off weight of *4600kg*. It is powered by PT6A-21 turboprop engines with Avia AV-844 propellers.
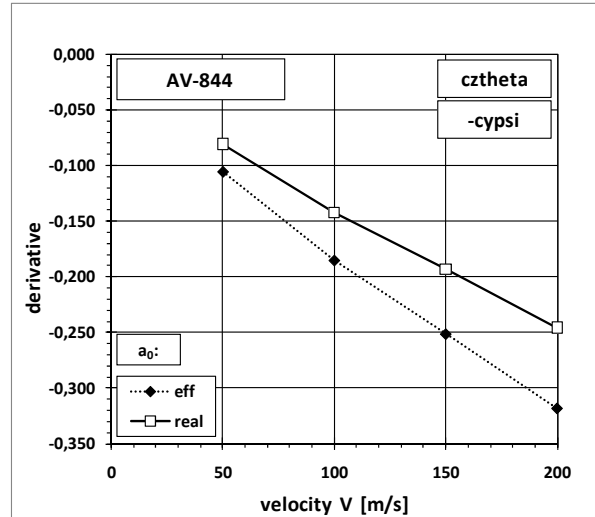
Fig. 4 Aerodynamic derivative $c_{z\Theta}$ - blade lift slope: a_{0eff}; $a_0(\eta)$
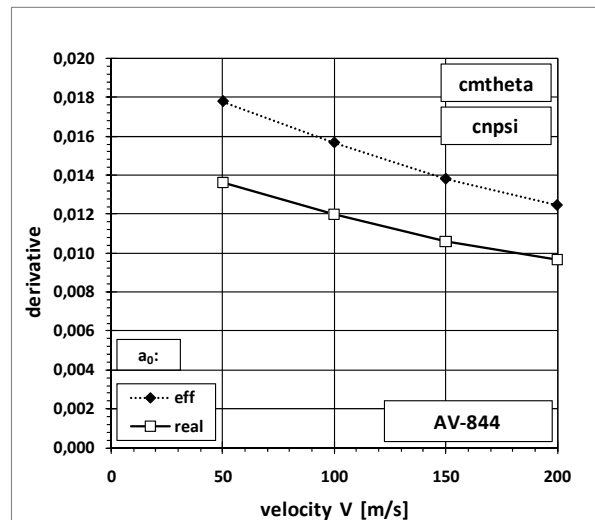
Fig. 5 Aerodynamic derivative $c_{m\Theta}$ - blade lift slope: a_{0eff}; $a_0(\eta)$

Firstly the evaluation of the aerodynamic derivatives is provided. The subjected AV-844 is 4-blade constant speed propeller with the diameter of *R = 1.041m*. The blade lift curve slope spanwise distribution as well as the geometry of the blade cannot be reproduced here. The effective value extracted by means of the *RMS* method of $a_{0eff} = 6.2478$ is slightly lower comparing to the profile theoretical value of 2π. Therefore the variance of derivatives considering 2π and a_{0eff} is barely noticeable. Figs. 4-6 show the examples of values of aerodynamic derivatives depend on the flow velocity considering a_{0eff} and $a_0(\eta)$.

World Academy of Science, Engineering and Technology
International Journal of Aerospace and Mechanical Engineering
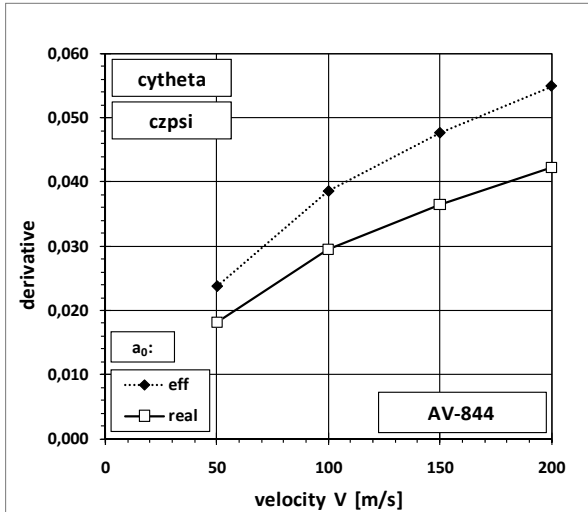Vol:8, No:4, 2014

Fig. 6 Aerodynamic derivative $c_{y\Theta}$ - blade lift slope: a_{0eff} ; $a_0(\eta)$

It is obvious from Figs. 4-6 that the derivatives considering the real blade lift slope distribution are lower comparing to those ones using the effective value. This fact hold true also for the other ones which are not shown here.

The final evaluation of the whirl flutter speed was performed using the NASTRAN program system supported by the in-house PROPFM software code. The detailed description of the analytical procedure by means of both standard and optimization solutions is provided e.g. in [11] and is not reproduced here as well as the detailed description of the EV-55M aircraft aeroelastic analyses that can be found e.g. in [12]. The structural model of the EV-55M is shown in Fig. 7 whereas the aerodynamic mesh is shown in Fig. 8.
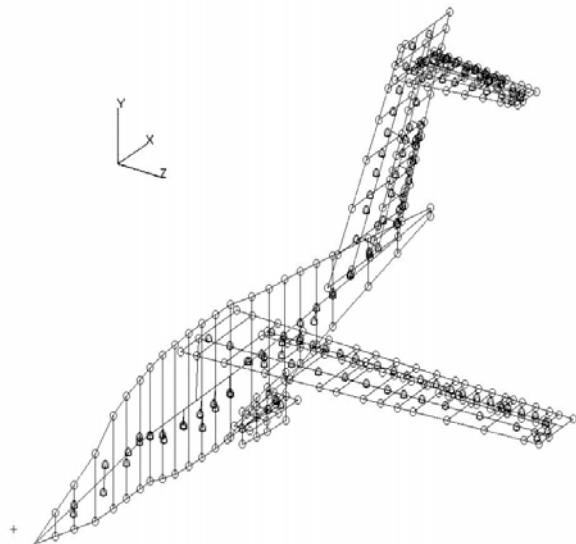

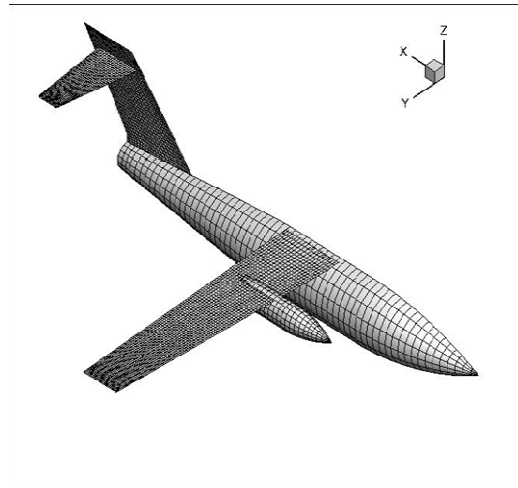Fig. 7 EV-55M aircraft structural FE model
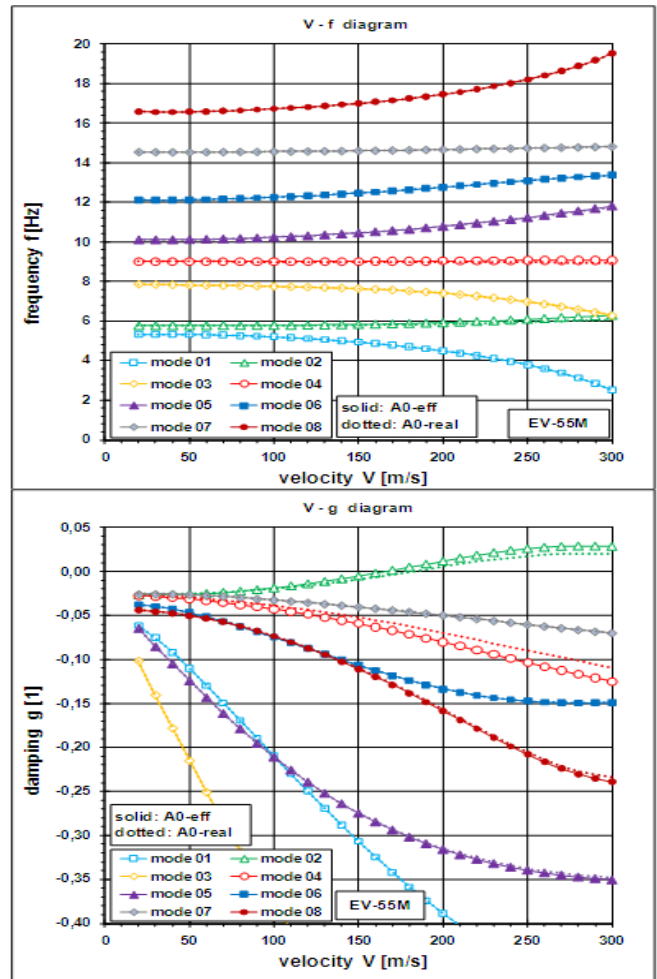

Fig. 8 EV-55M aircraft aerodynamic model

Fig. 9 V-g-f diagram - EV-55M aircraft - engine mount stiffness reduced by 50% - blade lift slope: a_{0eff} ; $a_0(\eta)$

The selected mass configuration of the structure includes *50%* of fuel, 2 passengers in the 3rd row and statically balanced controls. For the standard analysis the effective stiffnesses of the engine mount in both vertical and lateral

World Academy of Science, Engineering and Technology
International Journal of Aerospace and Mechanical Engineering
Vol:8, No:4, 2014

directions were reduced by *50%* in order to reach the critical state within the reasonable velocity range. The resulting *V-g-f* (velocity - damping - frequency) diagram is presented in Fig. 9. The solid lines with markers show the analysis using the effective value of the propeller lift curve slope whereas the dotted lines show the analysis using the real distribution of the lift curve slope.

There is the backward whirl flutter indicated on the mode *#2* that is the engine vertical vibrations mode. As expected there is the visible difference in the *V-g* curve of the modes *#2* and *#4* which are the engine vertical and lateral vibration modes, otherwise the differences are very small. Considering the effective value of the lift curve slope the flutter speed is $V_{FL} = 166.6$ [m.s^{-1}] whereas considering the real lift curve slope distribution the flutter speed become *$V_{FL} = 182.0$ [m.s^{-1}]*. It represents the increase in the flutter speed by *9.2%*. The flutter frequency was *$f_{FL} = 5.8$ [Hz]*, the difference between both cases was barely noticeable.

Further explanation of the blade lift slope influence on the whirl flutter characteristics is provided in Fig. 10. It shows the stability margins for the specific flutter velocity that together with the corresponding altitude represents the certification point according the (*V - H*) envelope. The margins which are calculated using the optimization approach of the whirl flutter analysis [11] define the critical values of the structural parameters (e.g., vertical and lateral engine vibration modes frequencies) in order to reach the required flutter speed. Again the real distribution of the lift curve slope gives the lower critical frequencies and thus higher reserve in terms of the whirl flutter stability with respect to the nominal state. The differences between both margins are ranging within (5.5-7.1)%. On the other side it should be noted that the effective value of the lift curve slope represents the conservative estimation.
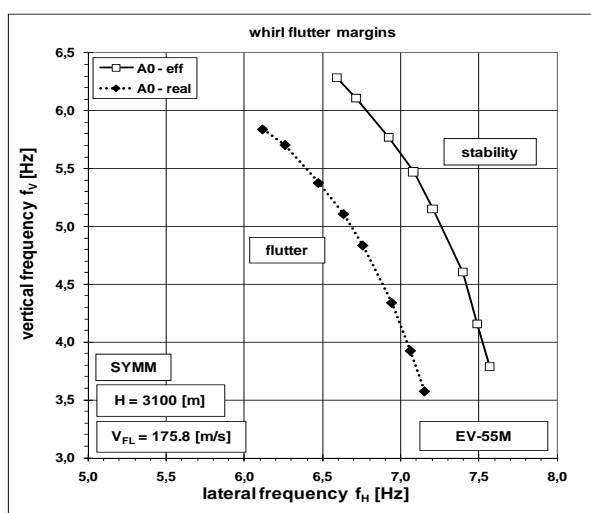

Fig. 10 Whirl flutter stability margins - blade lift slope: a_{0eff} ; $a_0 (\eta)$

V. CONCLUSION

This paper deals with evaluation of the influence of the propeller blade lift spanwise distribution to the whirl flutter.

Evaluation includes the effective (spanwise constant) value of the blade lift curve slope and more accurate real (spanwise variable) distribution of the blade lift slope. The application examples include the calculations of the propeller aerodynamic derivatives and the whirl flutter calculations of the reference twin turboprop aircraft structure. The usage of the real lift curve slope distribution causes the decrease of the aerodynamic derivatives. Comparing to the usage of the effective value the derivatives may vary quite significantly. Decreasing of the aerodynamic derivatives makes the increase of the flutter speed or decrease the critical values of the structural parameters (engine attachment stiffness, natural frequencies of engine vibration modes). The example of the reference aircraft shows the increase of the whirl flutter speed by *9.2%* and decrease of the necessary frequencies of the engine vibration modes by *(5.5-7.1)%*.

To conclude the usage of the real propeller blade lift curve slope distribution increases the accuracy of the results and raises the rate of reserve in terms of the flutter stability. It may be useful, e.g., considering the failure states that are required to be analyzed by the regulation standards. The usage of the effective value gives the conservative results, therefore, it would be applicable as well. However, with regard to the fact, that the effective value is extracted from the spanwise distribution the usage lose the reason.

REFERENCES

[1] E. S. Tailor, K. A. Browne, "Vibration Isolation of Aircraft Power Plants", *Journal of Aeronautical Sciences*, Vol.6, Dec 1938, pp.43-49
[2] W. H. Reed, *Review of Propeller - Rotor Whirl Flutter*, NASA Technical Report, NASA TR R-264, 1967
[3] W. H. Reed, S. R. Bland, *An Analytical Treatment of Aircraft Propeller Precession Instability*, NASA, Technical Note, TN D-659, 1961
[4] T. Theodorsen, *General Theory of Aerodynamic Instability and the Mechanism of Flutter*, NACA Report 496, 1935
[5] B. Smilg, L. S. Wasserman, *Application of Three-Dimensional Flutter Theory to Aircraft Structures*, Army Air Force Technical Report No.4798, 1942
[6] H. S. Ribner, *Propellers in Yaw*, NASA Rep.820, 1945
[7] H. S. Ribner, *Formulas for Propellers in Yaw and Charts of the Side - Force Derivatives*, NACA Rep.819, 1945
[8] J. C. Houbolt, W. H. Reed, "Propeller Nacelle Whirl Flutter", *Journal of Aerospace Sciences*, Vol.29, Mar 1962, pp.333-346
[9] W. P. Rodden, T. L. Rose, "Propeller / Nacelle Whirl Flutter Addition to MSC/NASTRAN", *MSC World User's Conference*, Universal City, CA, USA, March 1989
[10] C. E. Hammond, H. L. Runyan, J. P. Mason, "Application of Unsteady Lifting Surface Theory to Propellers in forward Flight", *AIAA Paper 74-419*, 1974
[11] J. Cecrdle, "Analysis of Twin Turboprop Aircraft Whirl-Flutter Stability Boundaries", *Journal of Aircraft*, Vol.49, No.6, pp.1718 − 1725, Nov − Dec 2012, ISSN 0021-8669, E-ISSN 1533-1013
[12] J. Cecrdle, J. Malecek, O. Cerny, "Aeroelastic Analysis of Twin Turboprop Utility Aircraft", *Proceedings of the Institution of Mechanical Engineers, Part G: Journal of Aerospace Engineering*, May 2011, Vol.225 pp.585-594, ISSN 0954-4100, eISSN 2041-3025